Rescuing Tetracycline Class Antibiotics for the Treatment of Multidrug-Resistant *Acinetobacter baumannii* Pulmonary Infection

David M. P. De Oliveira,[a] Brian M. Forde,[b] Minh-Duy Phan,[a] Bernhard Steiner,[a] Bing Zhang,[c] Johannes Zuegg,[c] Ibrahim M. El-deeb,[d] Gen Li,[a] Nadia Keller,[a] Stephan Brouwer,[a] Nichaela Harbison-Price,[a] Amanda J. Cork,[a] Michelle J. Bauer,[b] Saleh F. Alquethamy,[e] Scott A. Beatson,[a] Jason A. Roberts,[b,f,g] David L. Paterson,[b] Alastair G. McEwan,[a] Mark A. T. Blaskovich,[c] Mark A. Schembri,[a] Christopher A. McDevitt,[e] Mark von Itzstein,[d] Mark J. Walker[a]

[a]The University of Queensland, School of Chemistry and Molecular Biosciences, Australian Infectious Diseases Research Centre, Brisbane, QLD, Australia

[b]The University of Queensland, UQ Centre for Clinical Research, Australian Infectious Diseases Research Centre, Brisbane, QLD, Australia

[c]The University of Queensland, Centre for Superbug Solutions, Institute for Molecular Bioscience, Brisbane, QLD, Australia

[d]Griffith University, Institute for Glycomics, Gold Coast, QLD, Australia

[e]The University of Melbourne, Department of Microbiology and Immunology, Peter Doherty Institute for Infection and Immunity, Melbourne, VIC, Australia

[f]Royal Brisbane and Women's Hospital, Departments of Pharmacy and Intensive Care Medicine, Brisbane, QLD, Australia

[g]University of Montpellier, Division of Anaesthesiology Critical Care Emergency and Pain Medicine, Nîmes University Hospital, Nîmes, France

Mark A. Schembri, Christopher A. McDevitt, Mark von Itzstein, and Mark J. Walker contributed equally to this work. Author order was settled via mutual agreement.

ABSTRACT *Acinetobacter baumannii* causes high mortality in ventilator-associated pneumonia patients, and antibiotic treatment is compromised by multidrug-resistant strains resistant to β-lactams, carbapenems, cephalosporins, polymyxins, and tetracyclines. Among COVID-19 patients receiving ventilator support, a multidrug-resistant *A. baumannii* secondary infection is associated with a 2-fold increase in mortality. Here, we investigated the use of the 8-hydroxyquinoline ionophore PBT2 to break the resistance of *A. baumannii* to tetracycline class antibiotics. *In vitro*, the combination of PBT2 and zinc with either tetracycline, doxycycline, or tigecycline was shown to be bactericidal against multidrug-resistant *A. baumannii*, and any resistance that did arise imposed a fitness cost. PBT2 and zinc disrupted metal ion homeostasis in *A. baumannii*, increasing cellular zinc and copper while decreasing magnesium accumulation. Using a murine model of pulmonary infection, treatment with PBT2 in combination with tetracycline or tigecycline proved efficacious against multidrug-resistant *A. baumannii*. These findings suggest that PBT2 may find utility as a resistance breaker to rescue the efficacy of tetracycline-class antibiotics commonly employed to treat multidrug-resistant *A. baumannii* infections.

IMPORTANCE Within intensive care unit settings, multidrug-resistant (MDR) *Acinetobacter baumannii* is a major cause of ventilator-associated pneumonia, and hospital-associated outbreaks are becoming increasingly widespread. Antibiotic treatment of *A. baumannii* infection is often compromised by MDR strains resistant to last-resort β-lactam (e.g., carbapenems), polymyxin, and tetracycline class antibiotics. During the ongoing COVID-19 pandemic, secondary bacterial infection by *A. baumannii* has been associated with a 2-fold increase in COVID-19-related mortality. With a rise in antibiotic resistance and a reduction in new antibiotic discovery, it is imperative to investigate alternative therapeutic regimens that complement the use of current antibiotic treatment strategies. Rescuing the efficacy of existing therapies for the treatment of MDR *A. baumannii* infection represents a financially viable pathway, reducing time, cost, and risk associated with drug innovation.

KEYWORDS *Acinetobacter*, antibiotic resistance, ionophores, tetracyclines

Infections caused by carbapenem-resistant *Acinetobacter baumannii* are disseminated globally and are associated typically with high rates of morbidity and mortality (1). Habitually occurring in patients with significant health care system contact, *A. baumannii* is a major causative agent of bloodstream infections (BSIs), acute bacterial skin and skin structure infections (ABSSI), urinary tract infections, and ventilator-associated pneumonia (VAP). Within intensive care unit (ICU) settings, *A. baumannii* is one of the most common causative agents of VAP and is associated frequently with poor patient outcomes (2, 3). During the ongoing COVID-19 pandemic, challenges faced by health care professionals have been further exacerbated by multidrug-resistant (MDR) and extensively drug resistant (XDR) *A. baumannii* outbreaks (4–7). Recent reports suggest that up to 80% of ICU-admitted COVID-19 patients required invasive mechanical ventilation (8). Among these patients, MDR *A. baumannii* has been identified as a frequent cause of secondary bacterial infection, associated with a 2-fold increase in COVID-19-related mortality (9).

The persistence of *A. baumannii* in nosocomial settings has been attributed largely to the pathogen's intrinsic ability to survive desiccation and exposure to disinfectants (10, 11). Moreover, *A. baumannii* demonstrates a high capability to develop resistance to multiple classes of antibiotics. In 2019, European resistance rates for invasive isolates resistant to three antimicrobial groups (fluoroquinolones, aminoglycosides, and carbapenems) exceeded 43% (12). In the United States during 2017, over 60% of isolates were resistant to all fluoroquinolones and extended-spectrum β-lactam class antibiotics, ampicillin-sulbactam combinations, and trimethoprim-sulfamethoxazole combinations (13). Treatment regimens encompassing broad-spectrum cephalosporins, β-lactam-β-lactamase inhibitor combinations, carbapenems, and tetracycline class antibiotics are common approaches used to treat antibiotic-susceptible *A. baumannii* infections (14–16). In the increasingly frequent scenario of resistance to the aforementioned agents, combination therapy incorporating tigecycline with the highly nephrotoxic antibiotic colistin remains a last-resort treatment option, to which resistance is now being reported (12, 17). The inability to provide patients with an adequate treatment strategy reduces the efficacy of patient care (13, 18).

We have reported previously that dysregulation of bacterial metal ion homeostasis breaks antibiotic resistance in select bacterial pathogens (19–21). Here, using the 8-hydroxyquinoline analog PBT2 [2-(dimethylamino) methyl-5,7-dichloro-8-hydroxyquinoline] (22, 23), we demonstrate that the disruption of metal homeostasis breaks resistance to tetracycline class antibiotics in carbapenem-resistant, MDR, and XDR *A. baumannii* clinical isolates *in vivo*, using murine wound and pulmonary infection models. PBT2 is an orally bioavailable hydroxyquinoline ionophore which mediates the transfer of zinc across biological membranes. Phase 2 clinical trials on PBT2 have been completed for neurodegenerative conditions in which once-daily oral dosing of 250 mg was generally safe and well tolerated when administered for up to 12 months (EURO, REACH, and IMAGINE clinical trials) (23–25). This study demonstrates the rescue of tetracycline class antibiotics, including tigecycline, which are commonly used to treat carbapenem-resistant *A. baumannii* infections.

RESULTS

Monotherapy or combination therapy with next-generation tetracycline class antibiotics (e.g., tigecycline) is often employed as a last-resort measure to treat MDR and XDR *A. baumannii* infections. Unfortunately, resistance to these antibiotics is now being reported, which significantly reduces patient treatment options (26, 27). To address this challenge, in accordance with the Clinical and Laboratory Standards Institute (CLSI) and the European Committee on Antimicrobial Susceptibility Testing (EUCAST) guidelines (28, 29), the combination of PBT2 $\pm$ zinc to disrupt resistance to tetracycline class antibiotics in the clinical MDR *A. baumannii* strains MS14413 (30), AB5075 (31), and PGC-204089 (clinical isolate from the Royal Brisbane Women's Hospital) and the XDR *A. baumannii* strain AB0057 (32) was investigated. All *A. baumannii* strains demonstrated resistance to either tetracycline, doxycycline, or tigecycline (Table 1). Upon addition of PBT2, susceptibility to tigecycline was observed for MS14413, AB0057, and PGC-204089; susceptibility to doxycycline was observed for

TABLE 1 PBT2 and zinc resensitize tetracycline-resistant MDR and XDR A. baumannii strains to tetracycline class antibiotics[a]

Tetracycline class antibiotic	MIC (μg/mL) by A. baumannii strain and treatment															
	MS14413				AB0057				PGC-204089				AB5075			
	PBT2, 0 μM; Zn, 0 μM	PBT2, 64 μM; Zn, 0 μM	PBT2, 0 μM; Zn, 8 μM	PBT2, 64 μM; Zn, 8 μM	PBT2, 0 μM; Zn, 0 μM	PBT2, 64 μM; Zn, 0 μM	PBT2, 0 μM; Zn, 32 μM	PBT2, 64 μM; Zn, 32 μM	PBT2, 0 μM; Zn, 0 μM	PBT2, 64 μM; Zn, 0 μM	PBT2, 0 μM; Zn, 8 μM	PBT2, 64 μM; Zn, 8 μM	PBT2, 0 μM; Zn, 0 μM	PBT2, 64 μM; Zn, 0 μM	PBT2, 0 μM; Zn, 32 μM	PBT2, 64 μM; Zn, 32 μM
Tetracycline	16	4–8	16	**2**	>128	16	>128	**1**	64	32	64	**2**	8	**0.5**	8	**0.5**
Doxycycline	4	**0.25**	4	**0.125**	16	8	16	**2**	4	**2**	4	**1**	**0.5**	**≤0.125**	**0.5**	**≤0.125**
Tigecycline	8	**0.5**	8	**0.25**	8	**2**	8	**2**	4	**1**	4	**0.5**	**1**	**≤0.125**	**1**	**≤0.125**

[a]Resistance to tetracycline, doxycycline, and tigecycline was assessed for MDR A. baumannii strains MS14413, PGC-204089, and AB5075 and XDR A. baumannii strain AB0057. MIC assays were undertaken in the absence (untreated) or presence of PBT2, zinc, or PBT2 + zinc. MIC values highlighted in bold indicate an antibiotic susceptible breakpoint (≤2 μg/ml) in accordance with EUCAST guidelines for antimicrobial sensitivity testing. Data represent the mean of 3 biological replicates (29).

MS14413 and PGC-204089; and susceptibility to tetracycline was observed for AB5075. Moreover, the addition of both PBT2 and zinc potentiated susceptibility, according to EUCAST breakpoints, to tetracycline, doxycycline, and tigecycline for MS14413, AB0057, PGC-204089, and AB5075 (Table 1).

As shown by the treatment of *A. baumannii* strains MS14413 and AB0057, the combination PBT2 + zinc in the presence of either tetracycline, doxycycline, or tigecycline was observed to be bactericidal, indicated by a >3-log reduction in viable bacteria over 24 h (Fig. 1A). Furthermore, PBT2 alone and PBT2 + zinc visibly altered bacterial cell morphology, increasing the membrane permeability properties of both *A. baumannii* MS14413 and AB0057, respectively (Fig. 1B and C; see Fig. S1 and S2 in the supplemental material). As evidenced through visible membrane indentations and bacterial cell rupture, these effects were further augmented by the presence of either tetracycline, doxycycline, or tigecycline (Fig. 1B; Fig. S1).

We next investigated the likelihood of resistance development following treatment with tetracycline class antibiotics and PBT2 + zinc using the MDR *A. baumannii* strain MS14413. During serial passage for a period of 30 days in the presence of PBT2 + zinc and tetracycline class antibiotics, *A. baumannii* MS14413 demonstrated an appreciable increase in the MIC to tetracycline, doxycycline, and tigecycline, ranging from 31- to 127-fold (Fig. 2A). A 15-fold increase in the MIC of the control antibiotic rifampicin was also observed over the same time period (see Fig. S3 in the supplemental material). Compared with PBT2 in the presence of tetracycline or doxycycline, the reduced level of resistance for PBT2 in the presence tigecycline is possibly attributed to the presence of the *N,N*,-dimethylglycylamido side chain of tigecycline which has been associated with a decreased susceptibility to tigecycline resistance development (33). Notably, resistance to tetracycline, doxycycline, or tigecycline in the presence of PBT2 + zinc imposed a fitness cost, as evidenced by reduced growth in cation-adjusted Mueller-Hinton broth (CA-MHB) and lower survival in the lungs of mice compared with wild-type *A. baumannii* MS14413 (Fig. 2B; see Fig. S4 in the supplemental material). Whole-genome sequencing (WGS) of mutants resistant to tetracycline class antibiotics in the presence of PBT2 + zinc identified the presence of multiple chromosomal differences compared with the MS14413 reference genome (see Table S1 in the supplemental material). Notably, for mutants resistant to tetracycline in the presence of PBT2 + zinc, WGS identified the presence of insertion sequence (IS) IS*Aba125* in the TetR-family system regulator gene *adeN* which regulates the expression of the resistance-nodulation-cell division (RND) pathway AdeIJK (34, 35) (see Fig. S5 in the supplemental material; Table S1). Although the expression of AdeIJK contributes to the intrinsic resistance of *A. baumannii* to tetracycline class antibiotics, high levels of expression have been associated with toxicity to the bacterial cell (36). For mutants resistant to doxycycline in the presence of PBT2 + zinc, WGS identified appreciable stepwise mutations beginning in biofilm-associated cell-surface protein A (*bapA*) (37) followed by insertion of IS*Aba1* in *adeS* (encoding the AdeS sensor kinase of the two-component AdeRS regulatory system which regulates the RND AdeABC efflux pump system), proceeded by subsequent insertion of IS*Aba125* in *adeN* (Fig. S5; Table S1). Mutations in the two-component regulator AdeRS have been shown previously to result in an overexpression of the RND efflux system AdeABC, leading to moderate increases in resistance to tetracycline class antibiotics (38, 39). Observed changes in *bapA* are likely attributable to variation in the repetitive region. Although the impact of these changes has not been determined fully, they could potentially contribute to elevated MICs. For mutants resistant to tigecycline in the presence of PBT2 + zinc, WGS identified a stepwise insertion of IS*Aba125* in *adeN* followed by an insertion of IS*Aba1* in *adeS* (Fig. S5; Table S1). These mutations, combined with the previously noted chromosomal differences, may help explain the temporal stepwise development of resistance.

PBT2 facilitates the direct permeation of zinc ions across biological membranes, independent of membrane protein-dependent transport pathways (19). PBT2 treatment of *A. baumannii* MS14413 increased the cellular content of zinc and copper and reduced magnesium. Notably, iron was not affected significantly (Fig. 3A). The effect of PBT2 on cellular copper was amplified by the presence of exogenous zinc, indicating broad metal ion dyshomeostatic impacts.
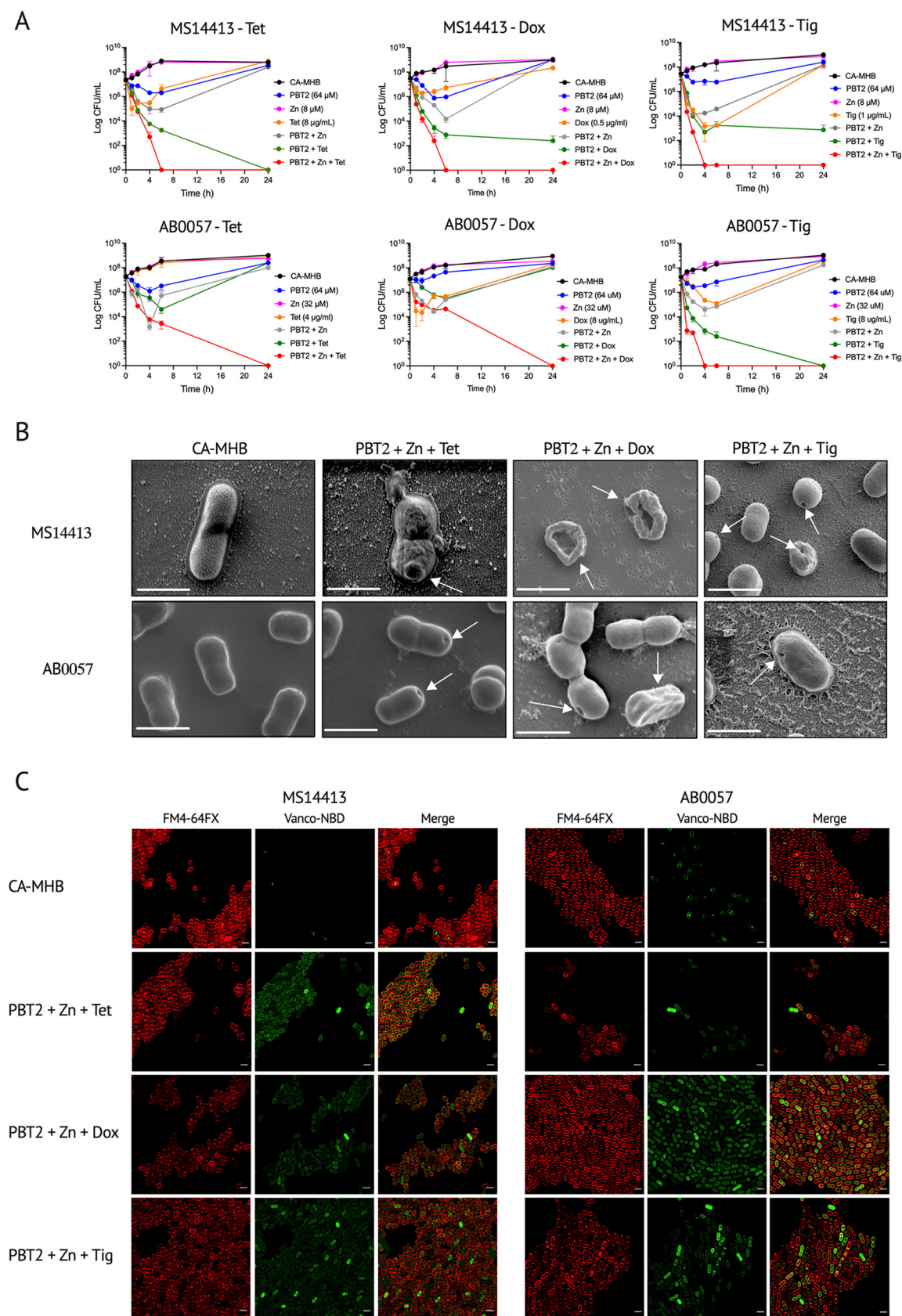
FIG 1 PBT2 + zinc in combination with tetracycline class antibiotics induces a bactericidal effect against tetracycline-resistant *A. baumannii*. (A) Time-kill curves for MDR *A. baumannii* strain MS14413 and XDR *A. baumannii* strain AB0057 in CA-MHB with or without PBT2, zinc, and
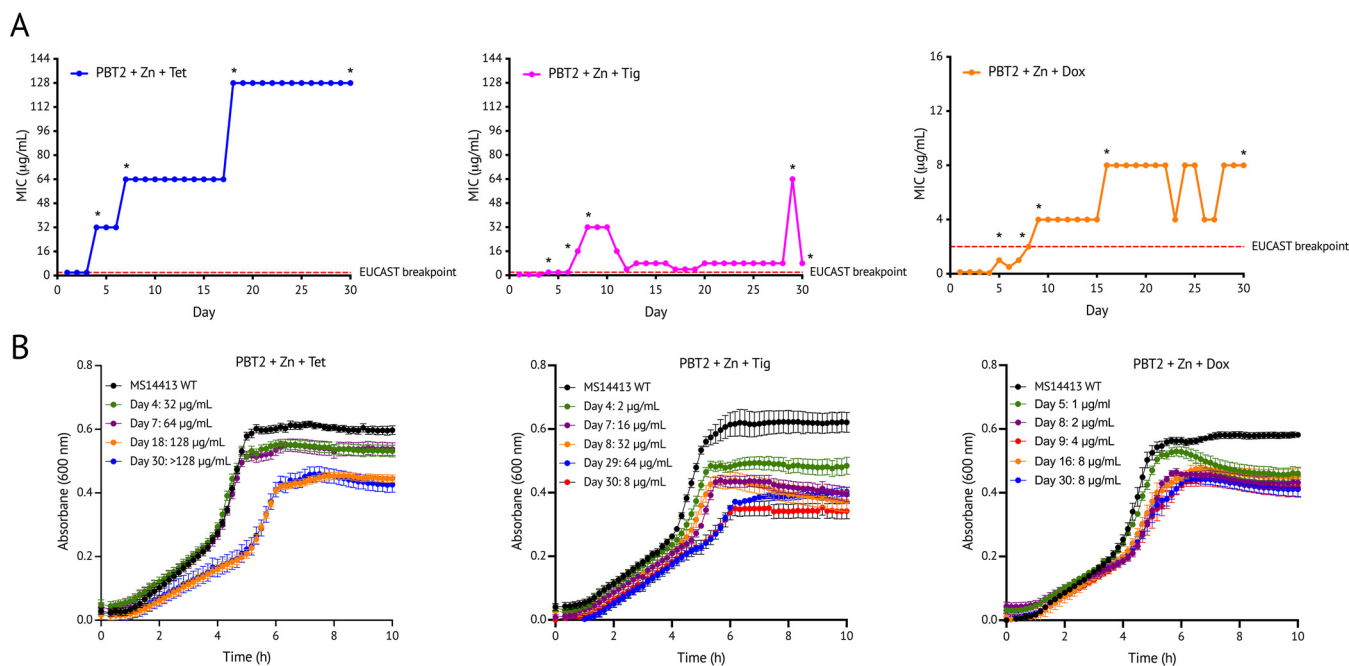
FIG 2 Resistance development against PBT2, zinc, and tetracycline class antibiotic combinations. (A) Development of resistance by *A. baumannii* strain MS14413 during serial passage with tetracycline, doxycycline, or tigecycline in the presence of subinhibitory concentrations of PBT2 and zinc in CA-MHB. Asterisks indicate time points where single colonies were isolated from a resistant culture. (B) Bacterial growth of resistant mutants (PBT2 + Zn + tetracycline class antibiotic) compared with that of wild-type (WT) *A. baumannii* MS14413. Growth curves are representative of three biological replicates.

Treatment of MS14413 with tetracycline class antibiotics alone had no direct effect on cellular metal content (Fig. 3A). To gain insight into the potential mechanism of action of PBT2 and zinc treatment, a transcriptome analysis of *A. baumannii* MS14413 was undertaken upon treatment with subinhibitory concentrations of PBT2, zinc, and tetracycline. Treatment with PBT2 was associated with changes in iron-specific metal stress response systems and drug efflux systems (Fig. 3B; see Table S2 in the supplemental material), which was confirmed by quantitative real-time PCR (Fig. 3C). Specifically, PBT2 led to the upregulation of iron uptake systems, including Feo system genes (*feoA* and *feoB*), ferric acinetobactin ABC transporter system genes (*bauC*, *bauD*, and *bauE*), and TonB receptor genes (*fpvA* and *pfeA*). Additionally, PBT2 exposure resulted in the upregulation of multidrug efflux resistance nodulation division transport system genes (*adeABC* and *adeFGH*) and downregulation of the small multidrug resistance (SMR) family drug efflux system gene *abeS*. No PBT2-dependent changes in the primary zinc, copper, or magnesium transport systems of *A. baumannii* were observed (40, 41) (Table S2). Nevertheless, the putative zinc exporting cation diffusion facilitator (CDF) gene *czcE* was upregulated suggesting zinc intoxication may be sensed by the bacterium (Table S2). These transcriptional changes were PBT2 dependent and were not affected by the presence of zinc or tetracycline (see Fig. S6 in the supplemental material; Table S2).

A. baumannii is a common cause of nosocomial ABSSI and VAP infections. An increase in the abundance of endogenous zinc at the site of infection is an important marker of bacterial wounds and lung infections (42–45). As such, we investigated the therapeutic potential of PBT2, in the absence of exogenous zinc, to break the resistance of *A. baumannii* MS14413

FIG 1 Legend (Continued)
tetracycline class antibiotics. Error bars indicate standard deviation from three biological replicates. (B) Scanning electron microscopy images of *A. baumannii* strains MS14413 and AB0057 grown in CA-MHB or in CA-MHB supplemented with PBT2 (64 μM) and zinc (8 μM for MS14413; 32 μM for AB0057) and either tetracycline (8 μg/mL for MS14413; 4 μg/mL for AB0057), doxycycline (0.5 μg/mL for MS14413; 8 μg/mL for AB0057), or tigecycline (1 μg/mL for MS14413; 8 μg/mL for AB0057) for 24 h at 37℃. Scale bars = 1 μm. Arrows indicate membrane indentations and membrane ruffling. (C) Confocal microscopy analysis of *A. baumannii* strains MS14413 and AB0057 grown in CA-MHB or in CA-MHB supplemented with PBT2 (64 μM) and zinc (8 μM for MS14413; 32 μM for AB0057) and either tetracycline (8 μg/mL for MS14413; 4 μg/mL for AB0057), doxycycline (0.5 μg/mL for MS14413; 8 μg/mL for AB0057), or tigecycline (1 μg/mL for MS14413; 8 μg/mL for AB0057) for 8 h at 37℃. Changes in bacterial membrane permeability were detected by staining bacteria with membrane-impermeable vancomycin-NBD fluorescent probe and membrane-labeling FM 4-64FX dye. Scale bars = 2 μm.
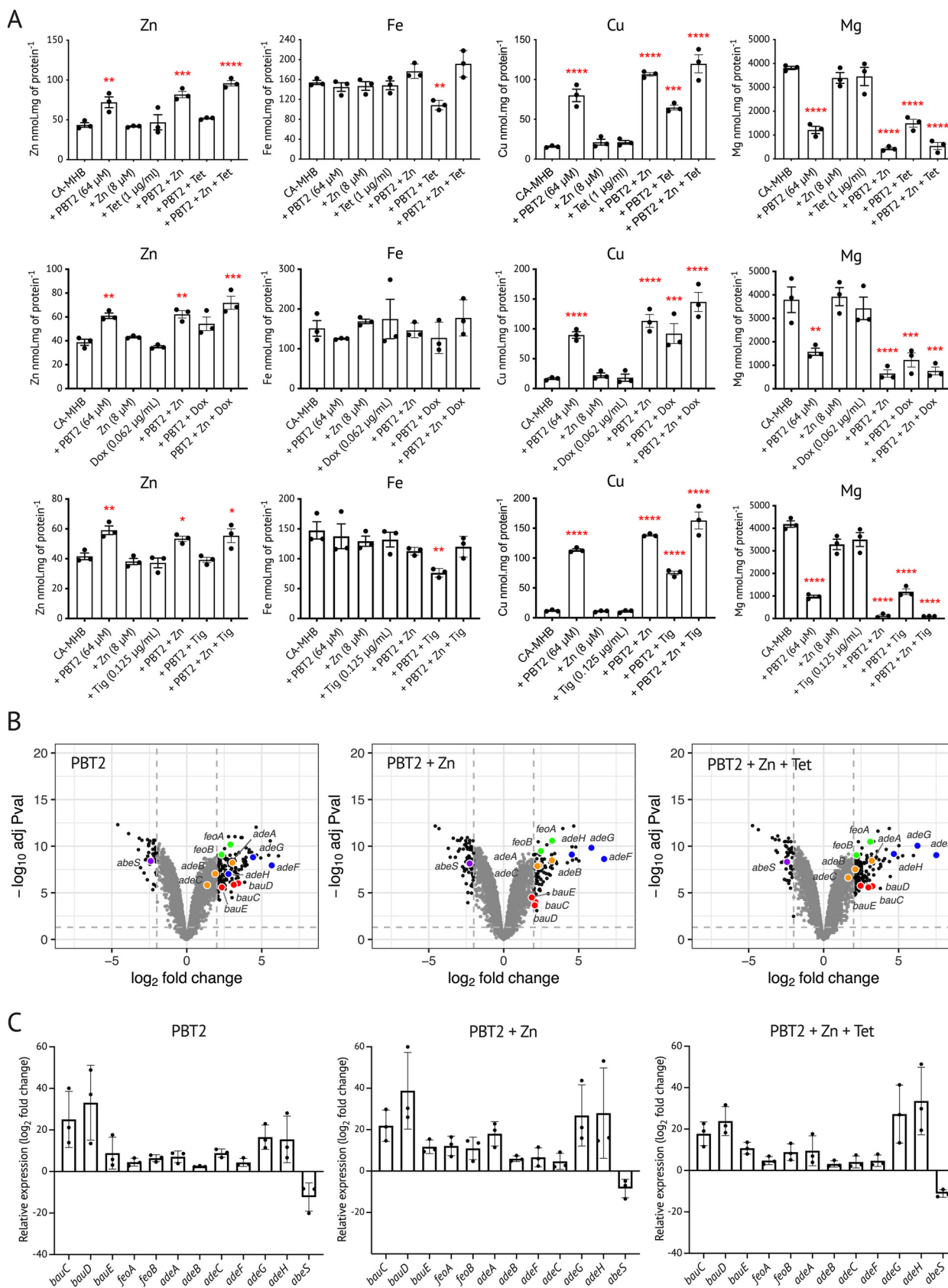
FIG 3 PBT2 dysregulates metal homeostasis in *A. baumannii* strain MS14413. (A) Whole cell zinc, iron, magnesium, and copper levels were assessed in *A. baumannii* strain MS14413 by inductively coupled plasma mass spectrometry. Bacteria were grown in CA-MHB in the absence or
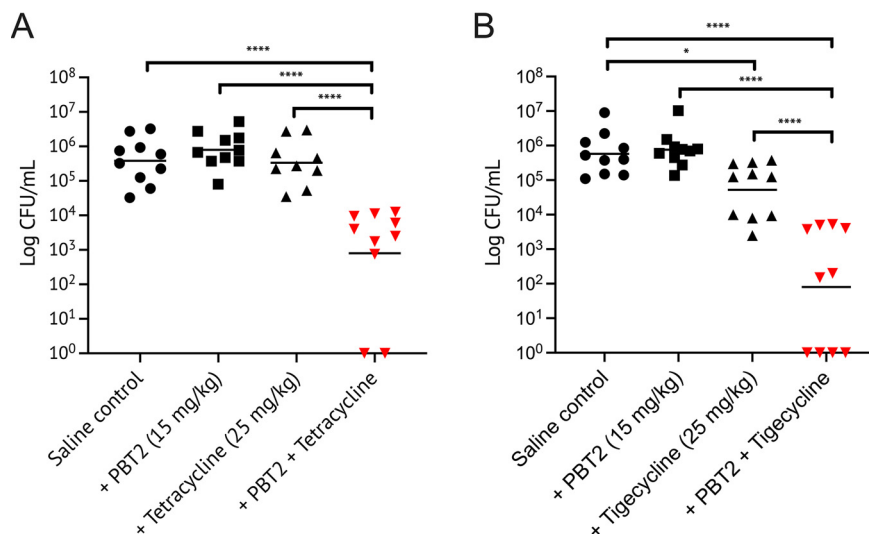
FIG 4 PBT2 breaks resistance to tetracycline class antibiotics in a pulmonary infection model. Cohorts of BALB/c mice ($n = 10$) were challenged intranasally with 1×10^8 CFU of MDR *A. baumannii* strain MS14413. CFUs were recovered from the lungs 24 h postchallenge. Mice were treated with combinations of PBT2 (15 mg/kg; oral gavage) and tetracycline (25 mg/kg; intraperitoneal injection) (A) or PBT2 (15 mg/kg; oral gavage) and tigecycline (25 mg/kg; intraperitoneal injection) (B) at 0 h and 6 h postinfection. Values for individual mice are plotted (*, $P \leq 0.05$; ****, $P \leq 0.0001$; one-way ANOVA with Tukey multiple comparisons).

to tetracycline class antibiotics *in vivo*. Using a murine model of ABSSI, treatment with PBT2, tetracycline, or tigecycline alone had no therapeutic effect. A significant therapeutic reduction in bacterial burden at the site of infection was observed only when PBT2 was used in combination with tetracycline or tigecycline (see Fig. S7 in the supplemental material). For lung infection, PBT2 treatment alone had no therapeutic effect, while tigecycline alone provided some therapeutic benefit. The combination treatment of PBT2 and tetracycline, or PBT2 and tigecycline, abrogated infection-associated weight loss in mice and resulted in significant 2.5-log and 4-log reductions in the bacterial burden in the lungs, respectively (Fig. S7; Fig. 4). Collectively, these data suggest that PBT2 may sequester zinc from the host niche, facilitating the rescue of tetracycline class antibiotics.

DISCUSSION

Carbapenem-resistant *A. baumannii* (CRAB) is a worldwide health concern, and CRAB resistance to last-resort therapies (i.e., polymyxin and tigecycline combination/monotherapy) has been reported (12, 17). Since 2018, only two new therapies have been approved by the U.S. Food and Drug Administration and/or the European Union European Medicines Agency for the treatment of CRAB infection, i.e., cefiderocol and eravacycline (1). Unfortunately, cefiderocol-nonsusceptible strains of CRAB emerged prior to initial U.S. FDA approval (46). Moreover, eravacycline was approved specifically for intra-abdominal infection and not serious BSI and VAP infections (1). The lack of financial drivers for the development and commercialization of new antibiotic therapies often outweighs the value to public health, and therefore, no investments are made for new therapies (47). As such, rescuing the efficacy of existing

FIG 3 Legend (Continued)

presence of PBT2, zinc, and tetracycline. Error bars indicate standard error of the mean from three biological replicates, *, $P \leq 0.05$; **, $P \leq 0.01$; ***, $P \leq 0.001$; ****, $P \leq 0.0001$; one-way ANOVA. (B) Volcano plots illustrating RNA-seq transcriptome analysis of *A. baumannii* strain MS14413 treated with either PBT2 (64 μM); PBT2 (64 μM) and zinc (8 μM); or PBT2 (64 μM), zinc (8 μM), and tetracycline (0.5 μg/mL) in CA-MHB. Genes with log$_2$ fold change of >2 or <−2 and a *P* value of <0.05 are depicted by black dots; Feo system genes (*feoA* and *feoB*) are depicted by green dots; ferric acinetobactin ABC transporter system genes (*bauC, bauD, and bauE*) are depicted by red dots; multidrug efflux resistance nodulation division transport system genes (*adeABC* and *adeFGH*) are depicted by orange and blue dots, respectively; SMR family drug efflux system gene *abeS* is depicted by the purple dot. Data were collected from three biological replicates. (C) Transcript levels for selected genes measured by quantitative real-time PCR. Log$_2$ fold changes were calculated relative to untreated controls and normalized to the *A. baumannii* reference gene *recA* using the $\Delta\Delta CT$ method. Error bars represent standard deviation of the mean of three biological replicates.

therapies for the treatment of serious bacterial infection represents a financially viable pathway, reducing time, cost, and risk associated with drug innovation.

Antibiotic potentiator molecules represent a promising avenue for rescuing the efficacy of existing antimicrobial therapies (48). In complex with zinc, ionophore compounds have been shown previously to potentiate polymyxin and amikacin activity against *A. baumannii in vitro* (19, 49). Here, we demonstrate that the ionophore PBT2 breaks *A. baumannii* resistance to tetracycline class antibiotics *in vivo*. Our data indicate that PBT2 broadly perturbs *A. baumannii* metal ion homeostasis resulting in a redistribution of metal ions within the cell with elevated zinc and copper and decreased intracellular magnesium. This generalized dysregulation of metal homeostasis increases the efficacy of tetracycline class antibiotics. While zinc accumulation can be explained by PBT2 treatment, the mechanistic basis for the increased copper levels remains speculative. This increase could also be mediated by PBT2, but the upregulation of two *cntO* orthologs, the TonB receptors for secreted bacterial metallophores, may suggest an alternative pathway. Cnt-type systems function analogously with broad-spectrum metallophores to compete for essential metals during infection (50). Although the biosynthetic pathway for a broad-spectrum metallophore in *A. baumannii* has yet to be defined, copper accumulation could be facilitated by such a pathway. Irrespective of the precise mechanistic basis, zinc and copper accumulation did not result in upregulation of the primary efflux systems *czcABC* and *copA*, respectively (40, 41). However, an increased expression of the CDF transporter *czcE*, which has been shown to be highly upregulated in response to zinc intoxication (41), was observed. Taken together, these data suggest that while the bacterium may sense the increased abundance of zinc, the overall levels of both metals are within the buffering capacity of the cell and do not trigger derepression of the major efflux systems. An alternative explanation may be that the elevated zinc and copper levels are disrupting the metalloregulatory systems that control expression of the efflux pathways. The decrease in cellular magnesium also failed to activate a starvation response. Bacterial sensing of magnesium levels differs from that of zinc and copper, which is normally achieved by the concerted action of a two-component regulator to sense extracellular magnesium and riboswitches to sense cytoplasmic magnesium (51, 52). Here, the availability of magnesium in the CA-MHB medium and the increased abundance of other divalent cations within the bacterium may explain the failure of *A. baumannii* to accurately sense magnesium depletion. Magnesium is a requisite cofactor in a wide variety of enzymes, and its depletion or displacement in both proteins and lipid scaffolds of the outer membrane by the increased abundance of zinc or copper could severely impact cellular viability (53). Magnesium is known to play a key role in maintaining the structural integrity of the lipopolysaccharide outer membrane of Gram-negative bacteria (54, 55). Through electrostatic interaction, magnesium binds to anionic phosphate groups of the inner core, enabling structural integrity of the outer leaflet. Disruptions in these important electrostatic cross-link interactions have been shown to result in lipopolysaccharide (LPS) release and subsequent bacterial membrane rupture (54, 56). Here, we hypothesize the PBT2-mediated depletion of cellular magnesium content may contribute to increased membrane permeability and associated membrane defects.

Unexpectedly, iron import [the Fe(II) import system Feo and the biosynthetic pathways for the Fe(III) siderophore acinetobactin] was upregulated in response to PBT2 treatment. It is possible that the upregulation of iron acquisition systems may be caused by PBT2-mediated movement of iron out of the cell or possibly mediated by displacement from metalloprotein sites by zinc or copper. Alternatively, the elevated iron scavenging response may be attributed to inappropriate sensing by iron-responsive regulators due to zinc or copper mismetallation. Iron is a crucial component of heme and iron-sulfur clusters, which are critical for respiratory enzymes in the electron transport chain and is an essential cofactor in a number of other cellular processes (57). Since *A. baumannii* is a nonfermentative bacterium that relies on respiratory electron transport, perturbation of iron homeostasis would have profound effects on cell physiology and metabolism.

Clinical trials have demonstrated that PBT2 is safe and well tolerated during use in humans (24). Here, we provide evidence that PBT2 potentiates tetracycline-class antibiotics

in vivo against MDR *A. baumannii* in a murine model of pulmonary infection. This study highlights the potential of PBT2 to be used in combination with tetracycline class antibiotics for the treatment of severe infection caused by drug-resistant *A. baumannii*.

MATERIALS AND METHODS

Materials. Tetracycline (catalog [cat.] no. 37919), doxycycline (cat. no. D9891), tigecycline (cat. no. PZ0021), and rifampicin (cat. no. R3501) were purchased from Sigma-Aldrich. PBT2 was produced by chemical synthesis (58), and the purity of the final product was confirmed to be >95% by ^{1}H and ^{13}C nuclear magnetic resonance (NMR), as described previously (21).

Bacterial strains, media, and growth conditions. *A. baumannii* strains MS14413 (30) AB0057 (32), AB5075 (31), and PGC-204089 (kindly provided by David L. Paterson) were grown in cation-adjusted Mueller-Hinton broth (CA-MHB) (cat. no. 212322, Becton Dickson) as per CLSI guidelines (28). Bacterial CFU enumeration was carried out on Luria Bertani broth (LB) agar. Bacteria were grown routinely at 37°C under aerobic conditions.

MIC determination. MICs and MIC breakpoints were determined by broth microdilution in accordance with CLSI/EUCAST guidelines as described previously (21, 28, 29). MIC assays were carried out in biological triplicate.

Bacterial time-kill assays. Bacteria were grown to an optical density at 600 nm (OD_{600}) of 0.4 in CA-MHB and treated with and without combinations of PBT2 (64 μM) and $ZnSO_4$ (8 μM for MS14413; 32 μM for AB0057) and either tetracycline (8 μg/mL for MS14413; 4 μg/mL for AB0057), doxycycline (0.5 μg/mL for MS14413; 8 μg/mL for AB0057), or tigecycline (1 μg/mL for MS14413; 8 μg/mL for AB0057) for 24 h at 37°C. To determine the rate of bacterial killing, aliquots of bacterial suspension were removed at 0, 1, 2, 4, 6, and 24 h; serially diluted in phosphate-buffered saline (PBS); and plated onto LB agar plates. Time-kill assays were performed in biological triplicate.

Scanning electron microscopy (SEM). SEM studies were undertaken at the Centre for Microscopy and Microanalysis at the University of Queensland. Bacterial strains were cultured in CA-MHB to an OD_{600} of 0.4 and treated in the absence and presence of PBT2 (64 μM) and $ZnSO_4$ (8 μM for MS14413; 32 μM for AB0057) and either tetracycline (8 μg/mL for MS14413; 4 μg/mL for AB0057), doxycycline (0.5 μg/mL for MS14413; 8 μg/mL for AB0057), or tigecycline (1 μg/mL for MS14413; 8 μg/mL for AB0057) for 24 h at 37°C. Bacteria were washed twice with PBS preceding glutaraldehyde fixation. Samples were then dehydrated, assisted with a Pelco biowave regimen, via a series of ethanol treatments (30% to 100% EtOH), with one treatment with 100% EtOH-hexamethyldisilazane (HMDS; 1:1), and finally two treatments with 100% HMDS. Samples were applied to coverslips coated with poly-L-lysine (1 mg/mL) before being air dried for 2 h. Coverslips were attached to 13-mm SEM stubs with double-sided carbon tabs, plasma cleaned for 10 min in an Evactron De-contaminator (XEI Scientific), and coated with two layers of platinum (first layer, 0° angle from above; second layer, 45° angle from above) using a Turbomolecular pumped coater (Quorum Tech) following the manufacturer's instructions. Samples were imaged in a JEOl JSM 7100F or JEOl JSM 7800F field emission SEM at an accelerating voltage of 1 to 3 kV.

Membrane permeability assay. From overnight cultures, *A. baumannii* strains MS14413 and AB0057 were diluted into fresh CA-MHB medium to an OD_{600} of 0.4. Bacteria were then treated in the absence or presence of PBT2 (64 μM) and $ZnSO_4$ (8 μM for MS14413; 32 μM for AB0057) with either tetracycline (8 μg/mL for MS14413; 4 μg/mL for AB0057), doxycycline (0.5 μg/mL for MS14413; 8 μg/mL for AB0057), or tigecycline (1 μg/mL for MS14413; 8 μg/mL for AB0057) for 8 h at 37°C. Approximately 4×10^8 CFU cells were then collected by centrifugation (3,200 $\times$ g, 2 min), and 500 μL of vancomycin-7-nitrobenzofurazan (NBD) fluorescent probe (59, 60) at 32 μg/mL was added to each sample and incubated for 30 min at 37°C with shaking (180 rpm). Bacteria were then labeled with 500 μL of FM 4-64FX (Thermofisher; cat. no. F34653) at 5 μg/mL (5 min on ice). For confocal microscopy, samples were then embedded on 1% agarose pads, and samples were analyzed on an inverted LSM 880 Fast Airyscan instrument (63$\times$/1.40 oil). For flow cytometric analysis, bacteria were then diluted with Hanks' balanced salt solution (Gibco) and analyzed on a CytoFlex S flow cytometer (Beckman Coulter). A fluorescein isothiocyanate (FITC) channel (excitation, 488 nm; emission, 525/40 nm) was used for the fluorescence intensity measurement of the vancomycin-NBD fluorescent probe, and 40,000 events were acquired per sample.

Resistance development studies. The development of resistance to tetracycline class antibiotics in the presence of PBT2 was undertaken as described previously (21). Briefly, *A. baumannii* MS14413 was sequentially passaged in subinhibitory concentrations of PBT2 + tetracycline class antibiotics over 30 days in CA-MHB. As a control for resistance development, the antibiotic rifampicin was used. Initially, the MIC for PBT2 with or without antibiotic was determined by broth microdilution following CLSI guidelines in a microtiter plate. The highest antibiotic or PBT2 + antibiotic concentration that still showed growth after overnight incubation was diluted 1:250 into a new microtiter plate containing 2-fold dilutions of antibiotic or PBT2 + antibiotic. This procedure was repeated for 30 days.

Genome sequencing analysis. DNA was extracted from overnight cultures of wild-type and mutant *A. baumannii* isolates resistant to tetracycline, doxycycline, or tigecycline in the presence of PBT2 + zinc using the DNeasy blood and tissue kit (Qiagen) as per the manufacturer's instructions. Paired-end Illumina DNA libraries were prepared using the Nextera DNA flex library prep kit (Illumina, Australia) with a modification of the starting input of 5 μL genomic DNA (gDNA) with samples of >20 ng/μL. WGS of pooled libraries was performed using the Illumina MiniSeq system and the high-output reagent kit (300 cycles). Illumina paired-end reads were assembled using SPAdes v3.14.1 (PMID 24093227) with default settings. Draft genome assemblies were ordered and orientated by aligning them to the complete genome of MS14413 using ragtag v1.1.0 (PMID 31661016). Pairwise alignments to MS14413 were visualized using the Artemis comparison tool (ACT) v18.1.0 (PMID

15976072). Whole-genome comparisons were then used to identify differences between wild-type and mutant MS14413 genomes. Insertion sequences were identified and annotated by a blastN comparison of draft genomes against the ISfinder database (PMID 16381877). Single nucleotide polymorphism (SNP) profiling and determination of core genome SNPs was undertaken by aligning the trimmed Illumina sequencing reads for each sample to the complete genome of wild-type strain MS14413 (GenBank accession CP054302) using Snippy v4.4.1 with a minimum read coverage of $10\times$ and minimum base quality of 20 that is required for a site to be considered.

Growth analysis. Overnight cultures of wild-type *A. baumannii* MS14413 and *A. baumannii* MS14413 resistant to PBT2 + tetracycline class antibiotics were standardized to an OD_{600} of 0.01 in CA-MHB medium. Bacteria were grown in a 96-well plate at a final volume of 200 μL and measured at 600 nm using a FLUOstar Omega microplate reader (BMG Labtech) at 37°C with shaking at 250 rpm. Growth assays were performed in biological triplicates and measured in technical triplicates.

PCR. PCR amplification of *adeN* and *adeS* genes in *A. baumannii* MS14413 were carried out using primers provided in Table S3 in the supplemental material.

ICP-MS. From overnight cultures, *A. baumannii* MS14413 was grown to an OD_{600} of 0.5 in CA-MHB. Cells were then treated with combinations of PBT2 (64 μM), $ZnSO_4$ (8 μM), and tetracycline (1 μg/mL) for 1 h at 37°C. Cells were harvested, processed, and analyzed using an Agilent 8900 ICP-QQQ instrument as described previously (21).

RNA isolation. RNA was isolated using a RNeasy Plus kit (Qiagen) as described previously (19). Briefly, *A. baumannii* MS14413 was grown to an OD_{600} of 0.5 in CA-MHB. Cells were then treated in the absence and presence PBT2 (64 μM), $ZnSO_4$ (8 μM), and tetracycline (1 μg/mL) for 1 h at 37°C. Two volumes of RNAprotect (Qiagen) were added to the cultures, and the samples were then centrifuged at 5,000 $\times$ *g* for 25 min at 4°C to pellet cells. RNA was isolated from the dry pellet as per the manufacturer's instructions. To ensure complete removal of DNA, the RNA was then further purified using the Turbo DNA-free kit (Thermo Fisher Scientific) according to the manufacturer's instructions.

Transcriptome sequencing (RNA-seq) analysis. RNA-seq analysis was performed at the Australian Genome Research Facility. The cDNA library was prepared and assessed as described previously (19). An average of 30 million reads per sample were generated, then trimmed using trimmomatic (v0.36), and mapped to the reference genome (*A. baumannii* MS14413 accession number NZ_CP054302) using bowtie2 (v2.3.4.2) with default parameters (–local –very-sensitive-local). Read counts were determined using featureCounts (Rsubread v1.28.1), and differential gene expression was analyzed with edgeR (v3.20.9) and limma-voom (v3.34.9) with the counts per minute (cpm) threshold set at 2.0. Figures were generated using ggplot2 (v3.3.0) and ggrepel (v0.8.2) packages in Rstudio (61).

Quantitative real-time PCR. Genes associated with heavy metal homeostasis were selected for quantitative real-time PCR analysis. Quantitative real-time PCR was carried out as described previously (19). Relative gene expression was calculated by the threshold cycle ($\Delta\Delta CT$) method using *recA* as the reference gene for *A. baumannii* MS14413. All experiments were done in biological triplicates and measured in technical triplicates. Primers used for quantitative real-time PCR are provided in Table S3.

Murine wound infection model. For wound infection, 7-week-old female BALB/c mice were prepared, anesthetized, and subjected to superficial scarification as described previously (21). For infection, *A. baumannii* MS14413 was cultured to mid-log phase in tryptic soy broth (TSB), and 1×10^6 CFU of bacteria was applied onto the scarified tissue in a final volume of 10 μL. Mice cohorts (*n* = 10) were treated with combinations of PBT2 (15 mg/kg of body weight; oral gavage), tetracycline (25 mg/kg; intraperitoneal injection), tigecycline (25 mg/kg; intraperitoneal injection), or saline solution (0.9%, wt/vol; intraperitoneal injection and/or oral gavage) in a 100-μL volume. Treatments were administered at 1, 6, 24, and 30 h postinfection. After 2 days of treatment, the mice were euthanized, the skin was excised, and bacteria were enumerated as described previously (19). Statistical differences in CFU were determined by a one-way analysis of variance (ANOVA), with a P value of <0.05 considered statistically significant (GraphPad Prism 9).

Murine pulmonary infection model. For pulmonary infection, cohorts of 7-week-old female BALB/c mice (*n* = 10) were challenged intranasally with a 25-μl preparation of 1×10^8 CFU of mid-log-phase *A. baumannii* MS14413 or mutant *A. baumannii* MS14413 resistant to PBT2 + tetracycline or PBT2 + tigecycline. For treatments, mice cohorts were treated with combinations of PBT2 (15 mg/kg; oral gavage), tetracycline (25 mg/kg; intraperitoneal injection), tigecycline (25 mg/kg; intraperitoneal injection), or saline solution (0.9% [wt/vol]; intraperitoneal injection and/or oral gavage) in a 100-μL volume. Treatments were administered at 0 and 6 h postinfection. At 24 h postinfection, mice were euthanized, and the lungs were harvested and washed in sterile PBS. To determine viable bacteria in the lungs, tissue was homogenized and plated as described previously.

Ethics. Animal experiments were performed according to the Australian code of practice for the care and use of animals for scientific purposes. Permission was obtained from the University of Queensland ethics committee (SCMB/AIBN/144/17).

Statistical analysis. All experiments were undertaken either in technical duplicate or triplicate, with no less than 3 biological replicates. Data are presented as means $\pm$ SD. Bacterial dissemination data from *in vivo* studies are presented as geometric means. To compare means between more than two groups, a one-way ANOVA with *post hoc* (Tukey) was conducted. Murine survival curves were analyzed using the Mantel-Cox log-rank test. Statistical analysis was performed using GraphPad Prism software v9. A P value of <0.05 was considered statistically significant.

Data availability. RNA-seq data sets generated and analyzed during the current study are available in the GEO repository (GSE175535). Genome data have been deposited to NCBI under BioProject PRJNA733838. Raw Illumina sequence read data have been deposited to the Sequence Read Archive (SRA) under the accessions SRR14695606, SRR14695607, SRR14695609 to SRR14695613, SRR14695615, SRR14695617, SRR14695618, and SRR14695620 to SRR14695625.

SUPPLEMENTAL MATERIAL

Supplemental material is available online only.

FIG S1, PDF file, 0.5 MB.

FIG S2, PDF file, 0.3 MB.

FIG S3, PDF file, 0.02 MB.

FIG S4, PDF file, 0.02 MB.

FIG S5, PDF file, 0.3 MB.

FIG S6, PDF file, 0.5 MB.

FIG S7, PDF file, 0.04 MB.

TABLE S1, DOCX file, 0.04 MB.

TABLE S2, DOCX file, 0.1 MB.

TABLE S3, DOCX file, 0.01 MB.

REFERENCES

1. De Oliveira DMP, Forde BM, Kidd TJ, Harris PNA, Schembri MA, Beatson SA, Paterson DL, Walker MJ. 2020. Antimicrobial resistance in ESKAPE pathogens. Clin Microbiol Rev 33:e00181-19. https://doi.org/10.1128/CMR.00181-19.

2. Ciginskiene A, Dambrauskiene A, Rello J, Adukauskiene D. 2019. Ventilator-associated pneumonia due to drug-resistant Acinetobacter baumannii: risk factors and mortality relation with resistance profiles, and independent predictors of in-hospital mortality. Medicina (Kaunas) 55:49. https://doi.org/10.3390/medicina55020049.

3. Chaari A, Mnif B, Bahloul M, Mahjoubi F, Chtara K, Turki O, Gharbi N, Chelly H, Hammami A, Bouaziz M. 2013. Acinetobacter baumannii ventilator-associated pneumonia: epidemiology, clinical characteristics, and prognosis factors. Int J Infect Dis 17:e1225–e1228. https://doi.org/10.1016/j.ijid.2013.07.014.

4. Perez S, Innes GK, Walters MS, Mehr J, Arias J, Greeley R, Chew D. 2020. Increase in hospital-acquired carbapenem-resistant Acinetobacter baumannii infection and colonization in an acute care hospital during a surge in COVID-19 admissions—New Jersey, February-July 2020. MMWR Morb Mortal Wkly Rep 69:1827–1831. https://doi.org/10.15585/mmwr.mm6948e1.

5. Baker S, Kellam P, Krishna A, Reece S. 2020. Protecting intubated patients from the threat of antimicrobial resistant infections with monoclonal antibodies. Lancet Microbe 1:e191–e192. https://doi.org/10.1016/S2666-5247(20)30126-9.

6. Clancy CJ, Schwartz IS, Kula B, Nguyen MH. 2021. Bacterial superinfections among persons with coronavirus disease 2019:A comprehensive review of data from postmortem studies. Open Forum Infect Dis 8:ofab065. https://doi.org/10.1093/ofid/ofab065.

7. Vijay S, Bansal N, Rao BK, Veeraraghavan B, Rodrigues C, Wattal C, Goyal JP, Tadepalli K, Mathur P, Venkateswaran R, Venkatasubramanian R, Khadanga S, Bhattacharya S, Mukherjee S, Baveja S, Sistla S, Panda S, Walia K. 2021. Secondary infections in hospitalized COVID-19 patients: Indian experience. Infect Drug Resist 14:1893–1903. https://doi.org/10.2147/IDR.S299774.

8. Maes M, Higginson E, Pereira-Dias J, Curran MD, Parmar S, Khokhar F, Cuchet-Lourenço D, Lux J, Sharma-Hajela S, Ravenhill B, Hamed I, Heales L, Mahroof R, Soderholm A, Forrest S, Sridhar S, Brown NM, Baker S, Navapurkar V, Dougan G, Bartholdson Scott J, Conway Morris A. 2021. Ventilator-associated pneumonia in critically ill patients with COVID-19. Crit Care 25:25. https://doi.org/10.1186/s13054-021-03460-5.

9. Li J, Wang J, Yang Y, Cai P, Cao J, Cai X, Zhang Y. 2020. Etiology and antimicrobial resistance of secondary bacterial infections in patients hospitalized with COVID-19 in Wuhan, China: a retrospective analysis. Antimicrob Resist Infect Control 9:153. https://doi.org/10.1186/s13756-020-00819-1.

10. Edwards J, Patel G, Wareham DW. 2007. Low concentrations of commercial alcohol hand rubs facilitate growth of and secretion of extracellular proteins by multidrug-resistant strains of Acinetobacter baumannii. J Med Microbiol 56:1595–1599. https://doi.org/10.1099/jmm.0.47442-0.

11. Farrow JM, Wells G, Pesci EC. 2018. Desiccation tolerance in Acinetobacter baumannii is mediated by the two-component response regulator BfmR. PLoS One 13:e0205638. https://doi.org/10.1371/journal.pone.0205638.

12. European Centre for Disease Prevention and Control. 2019. Surveillance of antimicrobial resistance in Europe: annual report of the European Antimicrobial Resistance Surveillance Network (EARS-Net) 2018. European Centre for Disease Prevention and Control, Stockholm, Sweden. https://www.ecdc.europa.eu/sites/default/files/documents/surveillance-antimicrobial-resistance-Europe-2018.pdf.

13. Centers for Disease Control and Prevention. 2019. Antibiotic resistant threats in the United States. https://www.cdc.gov/drugresistance/pdf/threats-report/2019-ar-threats-report-508.pdf.

14. Guillamet CV, Kollef MH. 2018. Acinetobacter pneumonia: improving outcomes with early identification and appropriate therapy. Clin Infect Dis 67:1455–1462. https://doi.org/10.1093/cid/ciy375.

15. Trecarichi EM, Quirino A, Scaglione V, Longhini F, Garofalo E, Bruni A, Biamonte E, Lionello R, Serapide F, Mazzitelli M, Marascio N, Matera G, Liberto MC, Navalesi P, Torti C, Pisani V, Costa C, Greco G, La Gamba V, Giancotti A, Barreca GS, Peronace C, La Valle O, Cimino G, La Torre P, Gemelli A, Tropea FA, Picicco F, Grp I, IMAGES Group. 2019. Successful treatment with cefiderocol for compassionate use in a critically ill patient with XDR Acinetobacter baumannii and KPC-producing Klebsiella pneumoniae: a case report. J Antimicrob Chemother 74:3399–3401. https://doi.org/10.1093/jac/dkz318.

16. Mei HK, Yang TL, Wang J, Wang R, Cai Y. 2019. Efficacy and safety of tigecycline in treatment of pneumonia caused by MDR Acinetobacter baumannii: a systematic review and meta-analysis. J Antimicrob Chemother 74:3423–3431. https://doi.org/10.1093/jac/dkz337.

17. Amat T, Gutierrez-Pizarraya A, Machuca I, Gracia-Ahufinger I, Perez-Nadales E, Torre-Gimenez A, Garnacho-Montero J, Cisneros JM, Torre-Cisneros J. 2018. The combined use of tigecycline with high-dose colistin might not be associated with higher survival in critically ill patients with bacteraemia due to carbapenem-resistant Acinetobacter baumannii. Clin Microbiol Infect 24:630–634. https://doi.org/10.1016/j.cmi.2017.09.016.

18. World Health Organization. 2017. Global priority list of antibiotic-resistant bacteria to guide research, discovery, and development of new antibiotics. http://www.who.int/medicines/publications/WHO-PPL-Short_Summary_25Feb-ET_NM_WHO.pdf?ua=1.

19. De Oliveira DMP, Bohlmann L, Conroy T, Jen FE, Everest-Dass A, Hansford KA, Bolisetti R, El-Deeb IM, Forde BM, Phan MD, Lacey JA, Tan A, Rivera-Hernandez T, Brouwer S, Keller N, Kidd TJ, Cork AJ, Bauer MJ, Cook GM, Davies MR, Beatson SA, Paterson DL, McEwan AG, Li J, Schembri MA, Blaskovich MAT, Jennings MP, McDevitt CA, von Itzstein M, Walker MJ. 2020. Repurposing a neurodegenerative disease drug to treat Gram-negative antibiotic-resistant bacterial sepsis. Sci Transl Med 12:eabb3791. https://doi.org/10.1126/scitranslmed.abb3791.

20. Jen FE, Everest-Dass AV, El-Deeb IM, Singh S, Haselhorst T, Walker MJ, von Itzstein M, Jennings MP. 2019. Neisseria gonorrhoeae becomes susceptible to polymyxin B and colistin in the presence of PBT2. ACS Infect Dis 6:50–55. https://doi.org/10.1021/acsinfecdis.9b00307.

21. Bohlmann L, De Oliveira DMP, El-Deeb IM, Brazel EB, Harbison-Price N, Ong CY, Rivera-Hernandez T, Ferguson SA, Cork AJ, Phan MD, Soderholm

AT, Davies MR, Nimmo GR, Dougan G, Schembri MA, Cook GM, McEwan AG, von Itzstein M, McDevitt CA, Walker MJ. 2018. Chemical synergy between ionophore PBT2 and zinc reverses antibiotic resistance. mBio 9: e02391-18. https://doi.org/10.1128/mBio.02391-18.

22. Cherny RA, Ayton S, Finkelstein DI, Bush AI, McColl G, Massa SM. 2012. PBT2 reduces toxicity in a *C. elegans* model of polyQ aggregation and extends lifespan, reduces striatal atrophy and improves motor performance in the R6/2 mouse model of Huntington's disease. J Huntingtons Dis 1:211–219. https://doi.org/10.3233/JHD-120029.

23. Lannfelt L, Blennow K, Zetterberg H, Batsman S, Ames D, Harrison J, Masters CL, Targum S, Bush AI, Murdoch R, Wilson J, Ritchie CW, group PEs. 2008. Safety, efficacy, and biomarker findings of PBT2 in targeting Abeta as a modifying therapy for Alzheimer's disease: a phase IIa, double-blind, randomised, placebo-controlled trial. Lancet Neurol 7:779–786. https://doi.org/10.1016/S1474-4422(08)70167-4.

24. Huntington Study Group Reach HDI. 2015. Safety, tolerability, and efficacy of PBT2 in Huntington's disease: a phase 2, randomised, double-blind, placebo-controlled trial. Lancet Neurol 14:39–47. https://doi.org/10.1016/S1474-4422(14)70262-5.

25. Villemagne VL, Rowe CC, Barnham KJ, Cherny R, Woodward M, Bozinovski S, Salvado O, Bourgeat P, Perez K, Fowler C, Rembach A, Maruff P, Ritchie C, Tanzi R, Masters CL. 2017. A randomized, exploratory molecular imaging study targeting amyloid beta with a novel 8-OH quinoline in Alzheimer's disease: the PBT2-204 IMAGINE study. Alzheimers Dement (N Y) 3:622–635. https://doi.org/10.1016/j.trci.2017.10.001.

26. He T, Wang R, Liu DJ, Walsh TR, Zhang R, Lv Y, Ke YB, Ji QJ, Wei RC, Liu ZH, Shen YB, Wang G, Sun LC, Lei L, Lv ZQ, Li Y, Pang MD, Wang LY, Sun QL, Fu YL, Song HW, Hao YX, Shen ZQ, Wang SL, Chen GX, Wu CM, Shen JZ, Wang Y. 2019. Emergence of plasmid-mediated high-level tigecycline resistance genes in animals and humans. Nat Microbiol 4:1450–1456. https://doi.org/10.1038/s41564-019-0445-2.

27. Asadi A, Abdi M, Kouhsari E, Panahi P, Sholeh M, Sadeghifard N, Amiriani T, Ahmadi A, Maleki A, Gholami M. 2020. Minocycline, focus on mechanisms of resistance, antibacterial activity, and clinical effectiveness: back to the future. J Glob Antimicrob Resist 22:161–174. https://doi.org/10.1016/j.jgar.2020.01.022.

28. Clinical and Laboratory Standards Institute. 2017. Performance standards for antimicrobial susceptibility testing, 27th edition. CLSI M100. Clinical and Laboratory Standards Institute, Wayne, PA.

29. European Committee on Antimicrobial Susceptibility Testing. 2019. Breakpoint tables for interpretation of MICs and zone diameters. https://www.eucast.org/fileadmin/src/media/PDFs/EUCAST_files/Breakpoint_tables/v_11.0_Breakpoint_Tables.pdf.

30. Roberts LW, Forde BM, Hurst T, Ling W, Nimmo GR, Bergh H, George N, Hajkowicz K, McNamara JF, Lipman J, Permana B, Schembri MA, Paterson D, Beatson SA, Harris PNA. 2021. Genomic surveillance, characterization and intervention of a polymicrobial multidrug-resistant outbreak in critical care. Microb Genom 7:mgen000530. https://doi.org/10.1099/mgen.0.000530.

31. Jacobs AC, Thompson MG, Black CC, Kessler JL, Clark LP, McQueary CN, Gancz HY, Corey BW, Moon JK, Si YZ, Owen MT, Hallock JD, Kwak YI, Summers A, Li CZ, Rasko DA, Penwell WF, Honnold CL, Wise MC, Waterman PE, Lesho EP, Stewart RL, Actis LA, Palys TJ, Craft DW, Zurawski DV. 2014. AB5075, a highly virulent isolate of *Acinetobacter Baumannii*, as a model strain for the evaluation of pathogenesis and antimicrobial treatments. mBio 5:e01076-14. https://doi.org/10.1128/mBio.01076-14.

32. Hamidian M, Venepally P, Hall RM, Adams MD. 2017. Corrected genome sequence of *Acinetobacter baumannii* strain AB0057, an antibiotic-resistant isolate from lineage 1 of global clone 1. Genome Announc 5:e00836-17. https://doi.org/10.1128/genomeA.00836-17.

33. Greer ND. 2006. Tigecycline (Tygacil): the first in the glycylcycline class of antibiotics. Proc (Bayl Univ Med Cent) 19:155–161. https://doi.org/10.1080/08998280.2006.11928154.

34. Rosenfeld N, Bouchier C, Courvalin P, Perichon B. 2012. Expression of the resistance-nodulation-cell division pump AdeIJK in *Acinetobacter baumannii* is regulated by AdeN, a TetR-type regulator. Antimicrob Agents Chemother 56:2504–2510. https://doi.org/10.1128/AAC.06422-11.

35. Hamidian M, Hancock DP, Hall RM. 2013. Horizontal transfer of an IS*Aba125*-activated *ampC* gene between *Acinetobacter baumannii* strains leading to cephalosporin resistance. J Antimicrob Chemother 68:244–245. https://doi.org/10.1093/jac/dks345.

36. Damier-Piolle L, Magnet S, Bremont S, Lambert T, Courvalin P. 2008. AdeIJK, a resistance-nodulation-cell division pump effluxing multiple antibiotics in *Acinetobacter baumannii*. Antimicrob Agents Chemother 52:557–562. https://doi.org/10.1128/AAC.00732-07.

37. Latasa C, Roux A, Toledo-Arana A, Ghigo JM, Gamazo C, Penades JR, Lasa I. 2005. BapA, a large secreted protein required for biofilm formation and host colonization of *Salmonella enterica* serovar Enteritidis. Mol Microbiol 58:1322–1339. https://doi.org/10.1111/j.1365-2958.2005.04907.x.

38. Sun JR, Perng CL, Chan MC, Morita Y, Lin JC, Su CM, Wang WY, Chang TY, Chiueh TS. 2012. A truncated AdeS kinase protein generated by IS*Aba1* insertion correlates with tigecycline resistance in *Acinetobacter baumannii*. PLoS One 7:e49534. https://doi.org/10.1371/journal.pone.0049534.

39. Lopes BS, Amyes SGB. 2013. Insertion sequence disruption of *adeR* and ciprofloxacin resistance caused by efflux pumps and *gyrA* and *parC* mutations in *Acinetobacter baumannii*. Int J Antimicrob Agents 41:117–121. https://doi.org/10.1016/j.ijantimicag.2012.08.012.

40. Alquethamy SF, Khorvash M, Pederick VG, Whittall JJ, Paton JC, Paulsen IT, Hassan KA, McDevitt CA, Eijkelkamp BA. 2019. The role of the CopA copper efflux system in *Acinetobacter baumannii* virulence. Int J Mol Sci 20:575. https://doi.org/10.3390/ijms20030575.

41. Alquethamy SF, Adams FG, Naidu V, Khorvash M, Pederick VG, Zang M, Paton JC, Paulsen IT, Hassan KA, Cain AK, McDevitt CA, Eijkelkamp BA. 2020. The role of zinc efflux during *Acinetobacter baumannii* infection. ACS Infect Dis 6:150–158. https://doi.org/10.1021/acsinfecdis.9b00351.

42. Botella H, Stadthagen G, Lugo-Villarino G, de Chastellier C, Neyrolles O. 2012. Metallobiology of host-pathogen interactions: an intoxicating new insight. Trends Microbiol 20:106–112. https://doi.org/10.1016/j.tim.2012.01.005.

43. McDevitt CA, Ogunniyi AD, Valkov E, Lawrence MC, Kobe B, McEwan AG, Paton JC. 2011. A molecular mechanism for bacterial susceptibility to zinc. PLoS Pathog 7:e1002357. https://doi.org/10.1371/journal.ppat.1002357.

44. Kambe T, Tsuji T, Hashimoto A, Itsumura N. 2015. The Physiological, biochemical, and molecular roles of zinc transporters in zinc homeostasis and metabolism. Physiol Rev 95:749–784. https://doi.org/10.1152/physrev.00035.2014.

45. Eijkelkamp BA, Morey JR, Neville SL, Tan A, Pederick VG, Cole N, Singh PP, Ong CLY, de Vega RG, Clases D, Cunningham BA, Hughes CE, Comerford I, Brazel EB, Whittall JJ, Plumptre CD, McColl SR, Paton JC, McEwan AG, Doble PA, Mcdevitt CA. 2019. Dietary zinc and the control of *Streptococcus pneumoniae* infection. PLoS Pathog 15:e1007957. https://doi.org/10.1371/journal.ppat.1007957.

46. Isler B, Doi Y, Bonomo RA, Paterson DL. 2019. New treatment options against carbapenem-resistant *Acinetobacter baumannii* infections. Antimicrob Agents Chemother 63:e01110-18. https://doi.org/10.1128/AAC.01110-18.

47. Theuretzbacher U, Outterson K, Engel A, Karlen A. 2020. The global preclinical antibacterial pipeline. Nat Rev Microbiol 18:275–285. https://doi.org/10.1038/s41579-019-0288-0.

48. Zurawski DV, Reinhart AA, Alamneh YA, Pucci MJ, Si YZ, Abu-Taleb R, Shearer JP, Demons ST, Tyner SD, Lister T. 2017. SPR741, an antibiotic adjuvant, potentiates the in vitro and in vivo activity of rifampin against clinically relevant extensively drug-resistant *Acinetobacter baumannii*. Antimicrob Agents Chemother 61:e01239-17. https://doi.org/10.1128/AAC.01239-17.

49. Magallon J, Chiem K, Tran T, Ramirez MS, Jimenez V, Tolmasky ME. 2019. Restoration of susceptibility to amikacin by 8-hydroxyquinoline analogs complexed to zinc. PLoS One 14:e0217602. https://doi.org/10.1371/journal.pone.0217602.

50. Ghssein G, Brutesco C, Ouerdane L, Fojcik C, Izaute A, Wang S, Hajjar C, Lobinski R, Lemaire D, Richaud P, Voulhoux R, Espaillat A, Cava F, Pignol D, Borezee-Durant E, Arnoux P. 2016. Biosynthesis of a broad-spectrum nicotianamine-like metallophore in *Staphylococcus aureus*. Science 352:1105–1109. https://doi.org/10.1126/science.aaf1018.

51. Groisman EA, Hollands K, Kriner MA, Lee EJ, Park SY, Pontes MH. 2013. Bacterial Mg^{2+} homeostasis, transport, and virulence. Annu Rev Genet 47:625–646. https://doi.org/10.1146/annurev-genet-051313-051025.

52. Ramesh A, Winkler WC. 2010. Magnesium-sensing riboswitches in bacteria. RNA Biol 7:77–83. https://doi.org/10.4161/rna.7.1.10490.

53. da Silva JJRF, Williams RJP. 2001. The biological chemistry of the elements: the inorganic chemistry of life, 2nd edition. Oxford University Press, Oxford, UK.

54. Clifton LA, Skoda MWA, Le Brun AP, Ciesielski F, Kuzmenko I, Holt SA, Lakey JH. 2015. Effect of divalent cation removal on the structure of Gram-negative bacterial outer membrane models. Langmuir 31:404–412. https://doi.org/10.1021/la504407v.

55. Schneck E, Schubert T, Konovalov OV, Quinn BE, Gutsmann T, Brandenburg K, Oliveira RG, Pink DA, Tanaka M. 2010. Quantitative determination of ion distributions in bacterial lipopolysaccharide membranes by grazing-incidence X-ray fluorescence. Proc Natl Acad Sci U S A 107:9147–9151. https://doi.org/10.1073/pnas.0913737107.

56. Marvin HJ, ter Beest MB, Witholt B. 1989. Release of outer-membrane fragments from wild-type *Escherichia coli* and from several *Escherichia coli*

lipopolysaccharide mutants by EDTA and heat-shock treatments. J Bacteriol 171:5262–5267. https://doi.org/10.1128/jb.171.10.5262-5267.1989.

57. Zhu Y, Zhao JX, Maifiah MHM, Velkov T, Schreiber F, Li J. 2019. Metabolic responses to polymyxin treatment in *Acinetobacter baumannii* ATCC 19606: integrating transcriptomics and metabolomics with genome-scale metabolic modeling. Msystems 4:e00157-18. https://doi.org/10.1128/mSystems.00157-18.

58. Barnham KJ, Gautier ECL, Kok GB, Krippner G. 2008. Preparation of 8-hydroxy-quinolines for treatment of neurological conditions. Patent US20080161353A1.

59. Blaskovich MAT, Phetsang W, Stone MRL, Lapinska U, Pagliara S, Bhalla R, Cooper MA. 2019. Antibiotic-derived molecular probes for bacterial imaging. Photonic Diagnosis and Treatment of Infections and Inflammatory Diseases II. SPIE BiOs, San Francisco, CA.

60. Blaskovich M, Cooper M, Butler M, Stone R, Phetsang W. 2018. Visualisation constructs. PCT patent application WO/2018/102890.

61. R Core Team. 2015. Integrated development for R. RStudio, Inc, Boston, MA.